fractal and fractional

MDPI

Article

Using Particle Swarm Optimization and Artificial Intelligence to Select the Appropriate Characteristics to Determine Volume Fraction in Two-Phase Flows

Abdullah M. Iliyasu [1,2,*], Abdallah S. Benselama [1], Dakhkilgova Kamila Bagaudinovna [3], Gholam Hossein Roshani [4,*] and Ahmed S. Salama [5]

1 Electrical Engineering Department, College of Engineering, Prince Sattam Bin Abdulaziz University, Al-Kharj 11942, Saudi Arabia
2 School of Computing, Tokyo Institute of Technology, Yokohama 226-8502, Japan
3 Department of Programming and Infocommunication Technologies, Institute of Mathematics, Physics and Information Technology, Kadyrov Chechen State University, 32 Sheripova Str., 364907 Grozny, Russia
4 Electrical Engineering Department, Kermanshah University of Technology, Kermanshah 6715685420, Iran
5 Faculty of Engineering and Technology, Future University in Egypt, New Cairo 11835, Egypt
* Correspondence: a.iliyasu@psau.edu.sa (A.M.I.); hosseinroshani@kut.ac.ir (G.H.R.)

Abstract: Global demand for fossil fuels has increased the importance of flow measurement in the oil sector. As a result, a new submarket in the flowmeter business has opened up. To improve the accuracy of gamma-based two-phase flowmeters, this study employs time-feature extraction methods, a particle swarm optimization (PSO) based feature selection system, and an artificial neural network. This article proposes a fraction detection system that uses a ^{137}Cs gamma source, two NaI detectors for recording the photons, and a Pyrex-glass pipe between them. The Monte Carlo N Particle method was used to simulate the geometry mentioned above. Thirteen time-domain features were extracted from the raw data recorded by both detectors. Optimal characteristics were identified with the help of PSO. This procedure resulted in the identification of eight efficient features. The input-output relationship was approximated using a Multi-Layer Perceptron (MLP) neural network. The innovation of the present research is in the use of a feature extraction technique based on the PSO algorithm to determine volume percentages, with results such as: (1) introducing eight appropriate time characteristics in determining volume percentages; (2) achieving an accuracy of less than 0.37 in root mean square error (RMSE) and 0.14 in mean square error (MSE) while predicting the volume fraction of components in a gas-liquid two-phase flow; and (3) reducing the calculation load. Utilizing optimization-based feature selection techniques has allowed for the selection of meaningful inputs, which has decreased the volume of computations while boosting the precision of the presented system.

Keywords: volume fraction; PSO technique; two-phase flow; artificial intelligence

check for updates

Citation: Iliyasu, A.M.; Benselama, A.S.; Bagaudinovna, D.K.; Roshani, G.H.; S. Salama, A. Using Particle Swarm Optimization and Artificial Intelligence to Select the Appropriate Characteristics to Determine Volume Fraction in Two-Phase Flows. *Fractal Fract.* **2023**, *7*, 283. https://doi.org/10.3390/fractalfract7040283

Academic Editor: Carlo Cattani

Received: 1 December 2022
Revised: 19 February 2023
Accepted: 16 March 2023
Published: 24 March 2023

Copyright: © 2023 by the authors. Licensee MDPI, Basel, Switzerland. This article is an open access article distributed under the terms and conditions of the Creative Commons Attribution (CC BY) license (https://creativecommons.org/licenses/by/4.0/).

1. Introduction

Studying the flow regime and the volume proportion of each component in multi-phase flows is a major area of focus in the oil, gas, and petroleum sectors. However, several techniques have been devised to ascertain these factors; these techniques may be categorized into two broad categories: those that include invasive procedures and those that do not. Many techniques such as: X-ray computer tomography; PIV modifications; MRI; Coriolis flowmeters; and speed cameras can be employed to study two-phase flow [1–3]. It has been demonstrated photon based techniques may be employed as a high accuracy non-destructive approach. Using a novel multi-energy gamma-ray attenuation method [4], Abouelwafa and Kendall set out to quantify the volumetric percentages of a three-phase flow for the first time. The accuracy of this method has been the subject of many recent investigations. In ref. [2], the gamma-ray technique has been used in static condition for metering the fraction of each phases. An experimental setup has been designed and three patterns, stratified, bubbly, and annular, have been produced. Using two detectors, unscattered photons have been registered and void percentage has been predicted by multilayer perceptron (MLP). In ref. [3], different flow patterns have been identified using radial basis function (RBF). Then, the void percentage of each pattern has been metered using three other different networks which is selected based on the pattern type. In ref. [4], different patterns have been simulated using MCNP code. The simulated structure consists of: a ^{137}Cs radiation source, a scattering detector, and a transmission detector. Three different features have been applied to the network, namely photons in Compton edge, scattered photons, and numbers of transmitted photons. Recently, many studies have been conducted to try to reduce the total number of detectors [5,6].

Peyvandi et al. [7] developed a unique framework to calculate the volume percentage of each component in a three-phase flow from just one pipe side. A gamma emitter radioisotope with an NaI detector placed close to it were implemented to register the gamma rays scattered from an object. The structures were implemented by Mayet et al. [8] to measure the gas percentage in two-phase flows regardless of changes in the flow pattern and the scale thickness in pipeline. Time and frequency-domain characteristics were reported by Hanus et al., to recognize the flow structure under dynamic settings [9,10]. Two ^{241}Am sources and a single scintillation detector were used in those investigations. Water-air fluxes were broken down into three possible shapes: a plug, a bubble, and a transitional plug-bubble. Time-domain data were employed by Hanus et al. [11] in conjunction with a different kind of artificial intelligence (AI) technique to recognize the flow regime. In the investigation discussed in ref. [12], ANN and PCA were implemented to recognize the flow pattern model under dynamic conditions. PCA was used to reduce the number of characteristics being looked at so that ANN could work better. Recent years have seen a plethora of research on the use of AI for the problem of gamma gauging [13,14]. Using an MLP neural network, Salgado and colleagues [15,16] were able to recognize the different flow regimes and estimate the volume fraction. Khayat et al., ran simulations of both annular and homogeneous flows at various volumes. After experimenting with several MLP ANN architectures, they were able to properly differentiate between flow regime types and calculate volumetric percentages with a root mean square error of less than 1.28 [17]. The flow regime was detected and volume fractions were reliably estimated using an ANN in ref. [18]. The analysis validated the use of both Computational Fluid Dynamics (CFD) and Monte Carlo algorithms. Ding Shao et al., calculated the gas volume fraction (GVF) of two-phase flow. In this study, data-driven models based on support vector machines (SVM) and neural networks were developed. The GVF of CO_2 could be dynamically measured using the permitted technique with an error of less than 16% [19].

Basahel and his coworkers used an X-ray tube and a sodium iodide detector to make predictions about the volume fractions and flow regimes. They used correlation analysis to examine temporal features that were extracted [20]. By analyzing the frequency characteristics of the recorded signals, researchers in ref. [21] attempted to recognize the kind of regime in three-phase flows. Two detectors were set up on the opposite end of the test pipe from the X-ray tube. The frequency characteristics of the received signals were collected after they were transformed into the frequency domain using FFT. Mayet and colleagues introduced a setup that used a dual-energy gamma source and a sodium iodide detector located on both sides of the test pipe to calculate the volumetric rate of petroleum products [22]. The ratios of four different pairings of petroleum products was measured by combining them in differing volume proportions. They used frequency data as inputs to a multilayer perceptron. Accuracy in oil pipeline control systems was a focus of the study presented in ref. [23], completed by extracting features using the wavelet transform from the received data. Although there are issues with using radioisotopes to determine multiphase flow characteristics, researchers have found that gamma-radiation-based methods are far more precise and dependable. Researchers have employed radioisotope equipment to measure a wide range of oil and gas sector variables. Studies [24–26] show that gamma sources can be applied to define the pattern and gas percentage of two-phase fluids, whereas studies [27–32] show that they can be used to establish the above mentioned parameters in the three-phase fluids. With two detectors, a pipe, and a ^{137}Cs radioisotope, Sattari et al. [30] proposed a framework in 2021. Many time characteristics were introduced and, using an MLP neural network, they determined the relationship between the extracted characteristics, the type of flow regimes, and volume percentages. Researchers aimed to streamline the detection process and cut down on the number of detectors needed in ref. [31]. To reduce the number of detectors, the researchers extracted several temporal features to apply to the GMDH neural network. Their accomplishments include a one-hundred-percent accurate categorization of flow regimes and a forecast of the void fraction percentage within the pipe less than 1.11 for root-mean-squared error (RMSE). Counts under the Compton continuum, photo peaks at 1.173 MeV and 1.333 MeV, and the average value of the signals collected by an NaI detector were all provided as acceptable features in another study [32]. The researchers used the aforementioned features as input to train a GMDH neural network, which was obtained by the MRE to predict volume percentages of 2.71%. Alamoudi et al., conducted research on how the thickness of the scales would affect the gas percentage of two-phase fluids [33]. Feature selection is a vital stage in classification preprocessing because it filters out unnecessary, redundant, and noisy data. The main benefits of a feature selection job include enhancing model performance, minimizing computing cost, and modifying the "curse of dimensionality". The issue space offers important information, but the development of the multi-objective-based feature selection algorithms also in use depends on the goal space. In order to rank the features based on their frequencies in the archive set, the authors of the article [34] suggest a multi-objective PSO-based approach called RFPSOFS. Then, the particles are directed by these rankings once the archive set has been refined. Another study was conducted in the field of the oil industry to determine the components of a three-phase fluids, in which the frequency and wavelet characteristics of the signals were investigated and useful characteristics were introduced using the PSO-based feature selection approach [35]. It is efficient and effective to predict bio-oil output using machine learning (ML) techniques [36]. The problem of using experimental methodologies to investigate the relationship between pyrolysis conditions, ultimate analysis, and proximate analysis with respect to bio-oil production is complex and difficult. Therefore, to accurately forecast the impact of input factors on bio-oil production, an effective and well-structured model must be developed. PSO and GA are used with a number of ML models to optimize the selection of features and hyperparameters.

Many of the aforementioned investigations suffer from a critical lack of feature selection and feature extraction methods that could be used to improve the performance of the AI. For this purpose, in this research, an attempt has been made to present a methodology for extracting time-domain features and selecting the effective characteristic based on the PSO algorithm. The proposed approach is demonstrated in Figure 1. Major contributions of the current research are listed below:

1. Extraction of time characteristics to determine volume percentages in two-phase fluids;
2. Including effective features employing an algorithm based on PSO algorithm for selecting features;
3. Significant increase in accuracy in determining volume percentages;
4. Selecting the most useful features as the neural network's input helps the system do fewer computations.

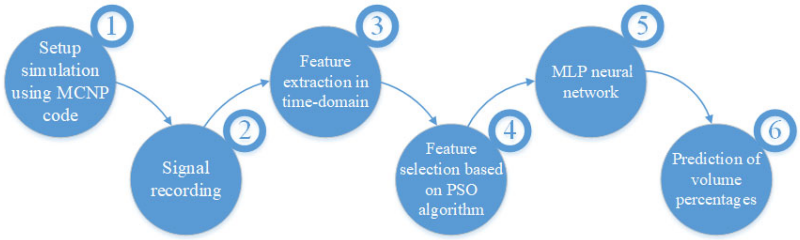

Figure 1. Flowchart of proposed methodology.

2. The Method of Simulation

These three environments (annular, stratified, and homogeneous) were simulated using the MCNP method in a static environment. Figure 2 illustrates a schematic of simulated regimes. Figure 3 depicts the simulation apparatus, which consists of a ^{137}Cs source and two detectors measuring 254 × 254 mm, positioned 250 mm from the source. In order to produce a wide beam, the collimator's opening angle has been set at 36°. Both the first and second detectors were positioned at an angle of 13° with regard to the source. Significant simulation work has been done before [3]. In that study, the optimal placement was found by maintaining one detector at an angle of 0° and varying the direction of the other detector from 7° to 18°. There is no mutual interference between detectors if they are set at an angle of 7° or more. The highest angle at which gamma rays may travel through the pipe and reach the second detector is 18°. Several volume fractions were simulated in each setting. This research demonstrated that the first and second detectors should be placed at an orientation of 0° and 13° with regard to the pipe's diameter, respectively, to minimize interference between the different flow regimes. Based on previous research [3], the detectors' position and orientation have been chosen for this investigation.

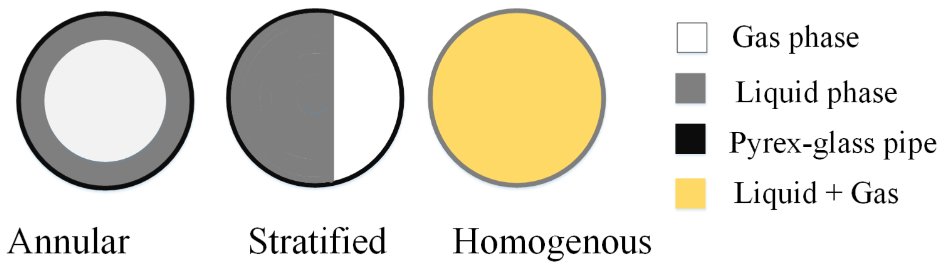

Figure 2. Simulated flow regimes.

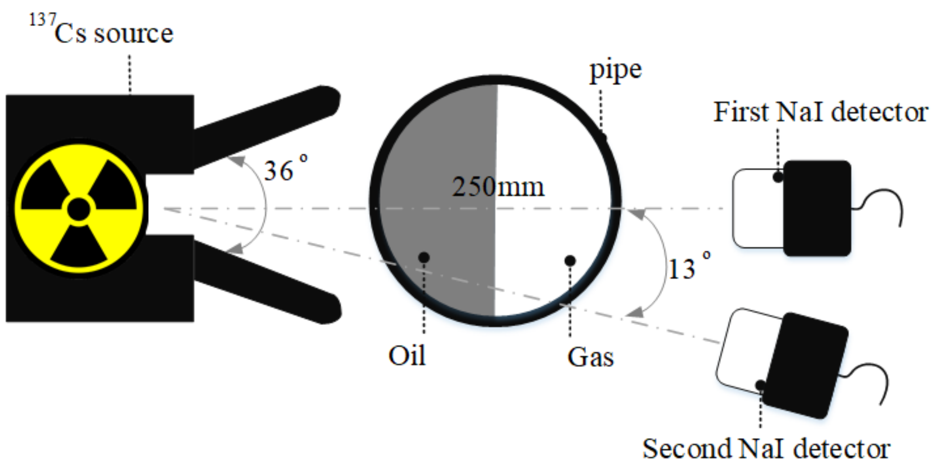

Figure 3. Model of the detecting system constructed using the MCNP code.

Gasoil (with the formula $C_{12}H_{23}$ and the density of 0.826 g/cm^3) and air (with the density of 0.00125 g/cm^3) were selected as the liquid and gas phases, respectively, for this investigation. All three flow patterns have been simulated 54 times, with each run simulating a void fraction ranging from 5% to 90% (with a step size of 5%). Multiple experiments performed in the prior study [3] confirm the structure being explored here. With several tests carried out in our earlier investigations, the structure under investigation in this study has been verified [3]. It was discovered that these outcomes follow each other by contrasting the simulated and measured output of the detectors. For the purpose of comparing the experimental and simulation data, both the simulated and measured results were normalized to the unit. A maximum relative discrepancy of 2.2% existed between the simulated and measured findings. The simulations and subsequent experiments were conducted in a static environment. While the real working environment is inherently dynamic, it could be conceptualized as static because of the set training reference points used by the flowmeter. The flowmeter was "trained" using these reference points to do volume fraction calculations, and to distinguish between flow regimes in a multi-phase flow meter in the operation. Multiphase oil, gas, and saltwater flow detection using gamma-ray neutron activation analysis was studied in ref. [20]. All of the simulations utilized in this work were first examined in a static environment before being applied to actual conditions. For the purpose of determining the salinity in the produced water, [21] the study analyzed transmitted and scattered gamma radiation. The simulations were all static, yet they were all employed in actual situations.

3. Signals Features Extraction

Figure 4 displays the data collected by two detectors for three different flow regimes. Data reduction, maintenance of the data's original properties, and improved interpretability are all achieved via feature extraction techniques. Features may be extracted in a variety of ways, including the time-domain, the frequency-domain, wavelet technique, and many more.

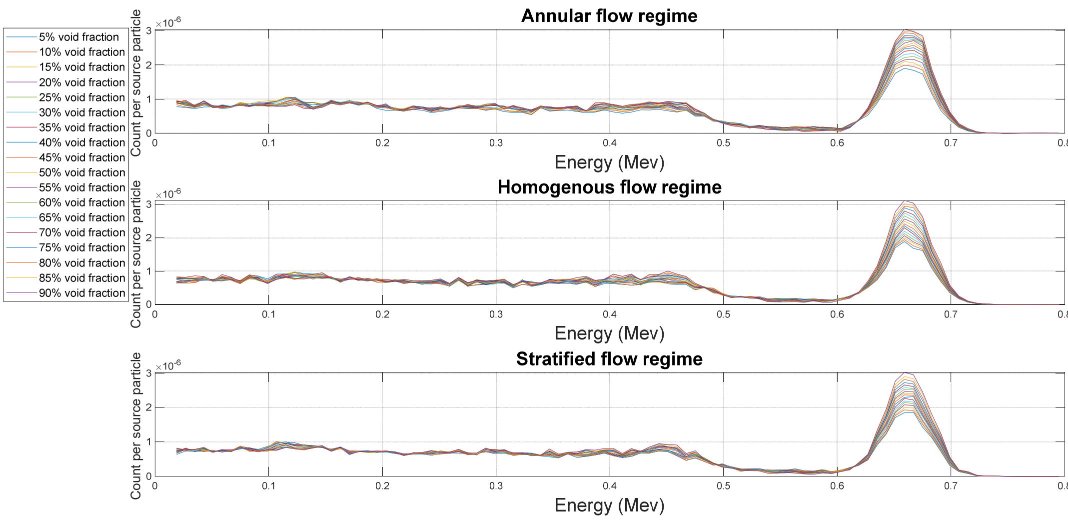

(**a**)

Figure 4. *Cont.*

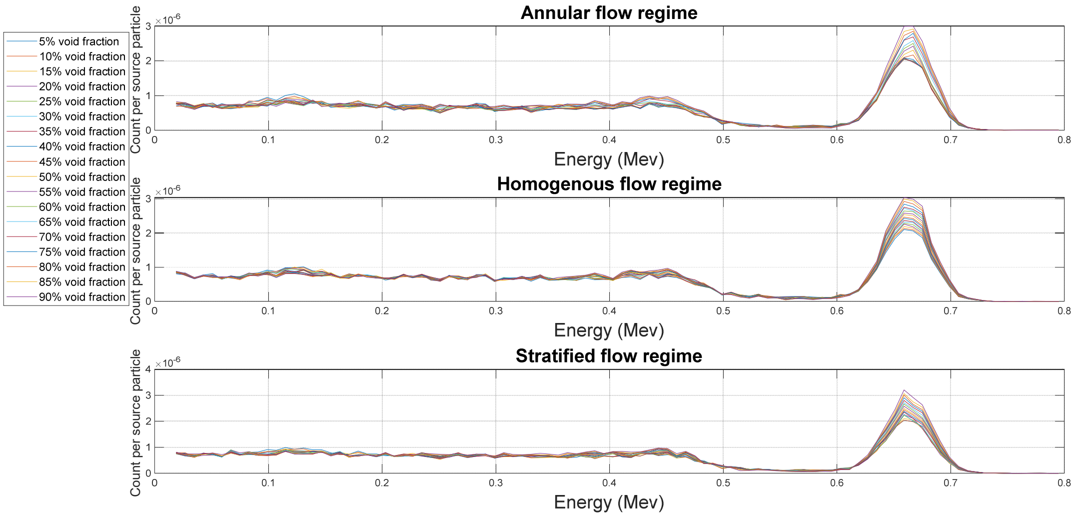

(**b**)

Figure 4. Recorded data from (**a**) first detector and (**b**) second detector for three annular, homogeneous, and stratified flow regimes.

- From the registered data of both detectors, thirteen time-domain characteristics were derived: (1) average value; (2) variance; (3) 4th order moment; (4) root mean square; (5) skewness; (6) kurtosis; (7) median; (8) waveform length (WL); (9) absolute value of the summation of square root (ASS); (10) mean value of the square root (MSR); (11) absolute value of the summation of the exp $^{\text{th}}$ root (ASM); (12) maximum value; and (13) standard deviation (STD) [30].

4. Feature Selection

This section assumes that there are N samples and M features in a labelled dataset (or attributes). Selecting G features (G $\leq$ M) from the initial feature set to get the best value for a particular performance cost function F(x) is, thus, a formulation of a Feature Selection (FS) issue. For instance, F(x) often stands for the estimation error in the prediction issue. It is possible to formulate a solution X for use in the FS procedure in the following form:

$$\begin{gathered} \mathrm{X} = (\mathrm{x}1, \mathrm{x}2, \ldots, x_M) \\ \mathrm{x_m} \in \{0, 1\} \qquad \forall_{\mathrm{m}} \in \{1, 2, \ldots, \mathrm{M}\} \end{gathered} \tag{1}$$

where the value of x_m indicates whether the feature in the mth dimension should be chosen or abandoned. As a result, the following formula describes an FS issue with M features:

$$\begin{gathered} \min F(X) \\ \text{s.t. } X = (x1, x2, \ldots, x_M) \\ x_m \in \{0, 1\}\ \forall_m \in \{1, 2, \ldots, \mathrm{M}\} \end{gathered} \tag{2}$$

Particle Swarm Optimization

Up to the present time, the PSO algorithm remains one of the most important programs used in the study of swarm intelligence [37]. The PSO algorithm has quickly risen to prominence in feature selection issues as a result of its efficacy and ease of use. This method is based on the group living strategies of real-world creatures, such as fish and birds. The algorithm relies on communication amongst all members of the population in order to find a solution. Each individual in the population is referred to as a "particle," and all of them are dispersed uniformly over the search space of the function being improved. The objective function is used to evaluate the location of each particle. Then, a direction of travel is selected by combining data from the current position, the best position it has ever been in, and the best particles in the collection. After every particle has reported its new location, the program moves on to the next stage. Iterating through these procedures several times ultimately yields the sought-after result. A flock of birds looking for food is analogous to a collection of particles looking for the greatest value of a function. This algorithm's main concept could be summarized in the following manner: particles change their position in the search space at each instant according to the best location they have seen so far and the best location among their neighbors. The PSO technique, like other evolutionary algorithms, starts with the creation of a completely random beginning population. N particles, chosen at random, make up the starting population. The location and velocity of a particle are represented by vectors of the same name. These particles begin to migrate in the problem space in search of better places when the value of the objective function is determined. Each particle must have two memories in order to do a search. Each particle's best historical position is recorded in one memory, as is the optimum location for all particles. Based on this data, the particles plan their next motion [37]. Each PSO particle represents a potential resolution to the problem. Two vectors are used to guide the search for the ith particle at each iteration: its location vector $X_i^t = [X_{i1}^t, X_{i2}^t, \ldots, X_{iD}^t]$; and its velocity vector $V_i^t = [V_{i1}^t, V_{i2}^t, \ldots, V_{iD}^t]$. Each particle's velocity and position are updated based on the best positions (or solutions) from two sources during motion: the particle's best position (denoted by by Sbesti = $[Sbest_{i1}, Sbest_{i2}, \ldots, Sbest_{iD}]$) and the best position from the population (denoted by Bbest = $[Bbest_1, Bbest_2, \ldots, Bbest_D]$). The ith particle's velocity and position are updated at the (t + 1)th iteration using the following calculations, which are based on Sbest and Bbest:

$$V_{id}^{t+1} = \omega * V_{id}^t + c_1 * r_1 * \left(Sbest_{id}^t - X_{id}^t\right) + c_2 * r_2 * \left(Bbest_d^t - X_{id}^t\right) \quad (3)$$

$$X_{id}^{t+1} = X_{id}^t + V_{id}^{t+1} \quad (4)$$

where t is the iteration number, ω is the inertia weight, c_1 and c_2 are acceleration constants known as the cognitive parameter and the social parameter, and r_1 and r_2 are uniformly distributed values in the range (0, 1). The value of different parameters used in the implemented PSO algorithm is shown in Table 1.

Table 1. Implemented PSO algorithm parameters.

No. of Iterations	30
Size of the Population	20
Inertia Weight	0.72
Inertia Weight Damping Ratio	1

One of the important elements of implementing optimization systems is defining the cost function. Considering that the PSO is an algorithm for solving continuous problems, to use this algorithm in a discrete problem, such as feature selection, we have first generated a continuous random key, and the location of this data (datum number) has been considered as a permutation. This permutation is set in such a way that the continuous data are sorted from the smallest to the largest, and are selected by considering the number of desired features from the beginning of this permutation. In other words, the trick used in this research was to use the location of continuous data as discrete data. The mean squared error (MSE) of a multilayer perceptron (MLP) neural network with a single hidden layer and 10 neurons in the hidden layer is used to calculate the cost function of the PSO system in this study. In this way, first, a number of inputs are randomly applied to the network from all the extracted characteristics, and the defined optimization system advances the inputs toward optimal inputs in order to reduce the defined cost function. PSO systems are designed in such a way that they attempt to forecast the goal using some identifying feature, and then gradually expand the number of inputs until the system is fully implemented across all possible modes. The cost function's value, as a function of the number of Inputs, is demonstrated in Figure 5. According to this figure, by choosing one input, the cost function's value is high, and with the increase in the number of entries, this value decreases. However, the point that is very important here is that by increasing the number of inputs to more than eight, the value of the cost function increases. Although the selection of 13 and 14 inputs has a small effect in reducing the cost function, this small effect cannot be considered due to the imposition of a large number of inputs to the system, and the selection of eight inputs was chosen as the most optimal mode. By checking the inputs, the characteristics of: 4th order moment; MSR; STD; skewness; ASS; mean value of signal recorded by the first detector and 4th order moment; and variance of the signal recorded by the second detector, have been introduced as 8 selected characteristics in the FS section:

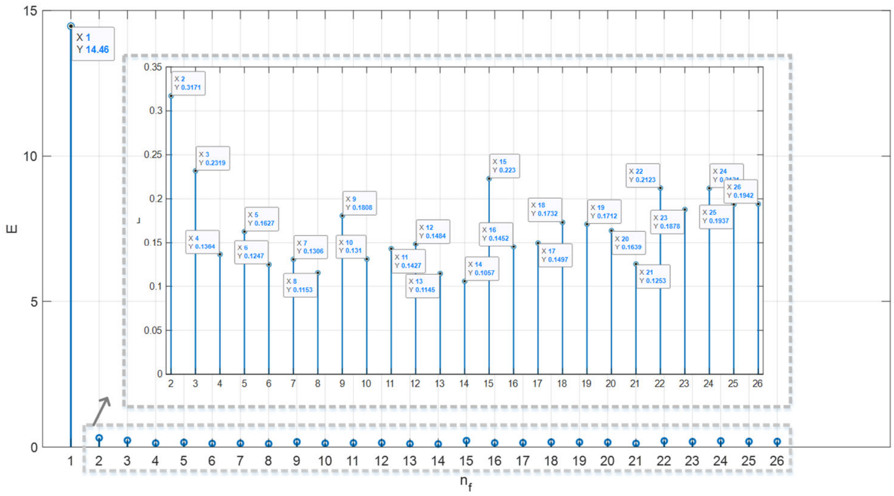

Figure 5. The cost function's value as a function of the number of inputs.

5. MLP Neural Network

Recently, a wide range of computational methods has been applied to specific problems in engineering research [38–60]. In this study, ANN was implemented to estimate the components of a two-phase flow. The most popular kind of ANN, multi-layer perceptron (MLP) models are employed in many applications. They learn the mappings between nonlinear functions and the many possible nonlinear decision surfaces. The following equations describe how to achieve neuron output in the output layer [61,62]:

$$n_l = \sum_{i=1}^{u} x_i w_{ik} + b \quad k = 1, 2, \cdots, m \tag{5}$$

$$u_j = f\left(\sum_{i=1}^{u} x_i w_{ik} + b\right) \quad k = 1, 2, \cdots, m \tag{6}$$

$$output = \sum_{n=1}^{j} (u_n w_n) + b \tag{7}$$

where x represents the input parameters, and b, w, and f denote the bias term, weighting factor, and activation function of the hidden layers. The input is indexed by i, while each hidden layer's neuron count is indexed by k. Present MLP networks are trained using the Levenberge Marquardt method, which uses the first and second derivatives (gradient and Hessian, respectively) to fine-tune the network's weights. A total of 38 samples are utilized in the training phase, 8 in the validation phase, and 8 in the testing phase. Patterns and examples make up the majority of the data needed to train a neural network. "Validation data" refers to the subset of the dataset which is implemented to evaluate the performance of the training procedure. As the last phase in the training process, the test data are given to the NN to ensure precise performance. A neural network will be resilient to function in a real situation if it performs well on the aforementioned dataset. This article uses MLP ANN models that have been trained to forecast the volume fraction. Many different ANN structure were implemented and optimized until one had the lowest error rate. Several arrangements with various hidden layers and neurons were analyzed.

6. Results

In this manuscript, a diagnostic instrument comprising two sodium iodide detectors, a cesium radioisotope, and a pipe under test were simulated with MCNP code. The angle between the two detectors was 13° to record the received signals with the least interference. Three different flow regimes were simulated at 18 different volume percentages. 13 temporal characteristics were extracted from the signals of two detectors, and a total of 26 characteristics were collected from all tests. The extracted features were given to the PSO-based feature selection algorithm to select the optimum mixture of them. Many PSO-based FS methods have been developed in recent decades [63–65].

After defining the efficient features, the MLP neural network was trained with these features to estimate the gas percentage inside the pipe. As depicted in Figure 6, this network has eight inputs, two hidden layers, and one output. The hidden layers' neurons are 15 and 10 neurons, respectively. Table 2 shows the implemented MLP specifications. To illustrate the network's efficacy throughout the training, validation, and testing datasets, Figure 7 includes two error and regression diagrams. The network's output (blue circles) and the desired outcome (black line) are shown in the regression diagram. The precision of the planned network is shown by their mutual compatibility. The error diagram graphically displays the deviation between target value and neural network's output. Two error criteria (named MSE and RMSE, respectively) for data in the training, validation, and testing stages were calculated. The maximum value of MSE and RMSE is equal to 0.14 and 0.37, respectively. Table 3 compares the capability of the provided system with that of earlier studies, demonstrating the impact of feature extraction on the precision of the volume percentage detection method. Useful characteristics were picked as inputs to the NN using the PSO-based approach, which allowed for the great accuracy attained in this study. The use of optimization methods in the selection of suitable features is the innovation of the current research, which has caused a significant reduction in the error in the volumetric percentage detection system.

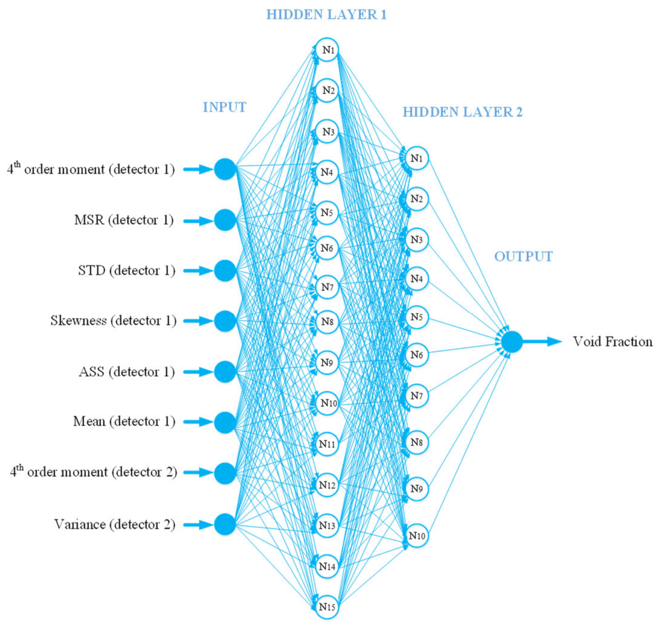

Figure 6. The neural network structure that was created to forecast the void fraction.

Table 2. Properties of the implemented network.

Type of Applied ANN	MLP
Nodes of input layer	8
Nodes of 1st hidden layer	15
Nodes of 2nd hidden layer	10
Nodes of output layer	1
Epochs	500
Activation function applied for any neuron	Tansig

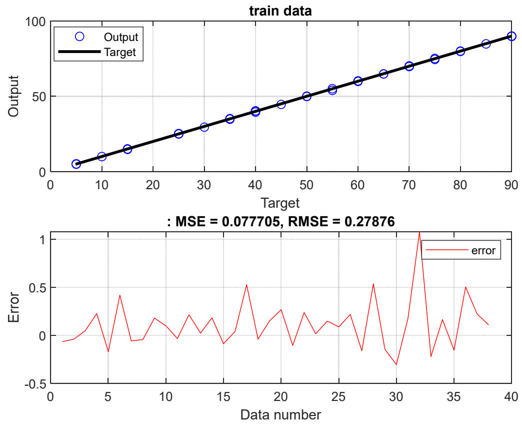

(**a**)

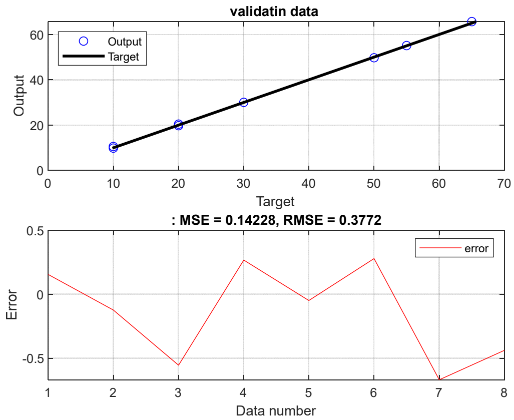

(**b**)

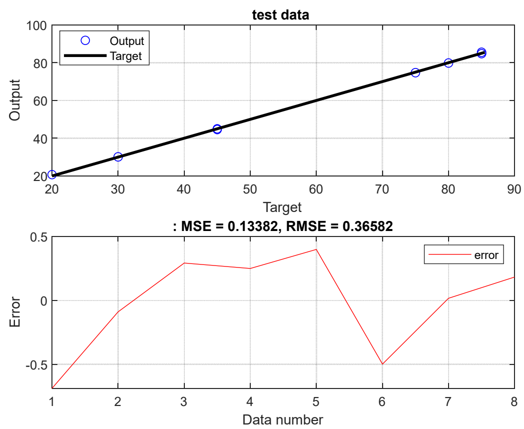

(**c**)

Figure 7. Results of the NN on three different types of data: (**a**) training, (**b**) validation, and (**c**) testing.

Table 3. Examination of the presented detection system's accuracy in light of related research.

Ref.	Method of Feature Extracted	Method of Feature Selection	Neural Network's Type	MSE	RMSE
[4]	Without feature extraction	Without feature selection	MLP	1.08	1.04
[6]	Without feature extraction	Without feature selection	RBF	37.45	6.12
[7]	Without feature extraction	Without feature selection	MLP	2.56	1.6
[26]	Frequency features	Without feature selection	MLP	0.67	0.82
[30]	Time features	Without feature selection	GMDH	1.24	1.11
[31]	Time features	Without feature selection	MLP	0.21	0.46
[32]	Without feature extraction	Without feature selection	GMDH	7.34	2.71
[current study]	Time features	PSO-based feature selection	MLP	0.14	0.37

7. Conclusions

Companies in the oil and gas sector have been motivated to explore novel avenues of development in search of more effective production methods by their insatiable want for fossil fuels. In this paper, a system using a ^{137}Cs gamma source, a Pyrex-glass, and two sodium iodide detectors for precise volumetric percentage determination in two-phase flows regardless of flow pattern is introduced. In all three flow regimes, simulated signals were recorded. From recorded signals, thirteen time-domain characteristics were extracted from two detectors, and a total of 26 features were available. PSO algorithm was used to find the most optimal characteristics, and the result of this algorithm was the introduction of eight characteristics as efficient features. A MLP neural network with two hidden layers, 15 and 10 neurons in the 1st and 2nd hidden layers, was responsible for transferring the input space (selected characteristics) to the output space (percentage of void fraction), which performed this task with RMSE of less than 0.37. The measurement precision of the system presented in this research was due to its efficient characteristics, which were due to the PSO algorithm. The use of different optimization algorithms regarding feature selection to increase accuracy and reduce the volume of calculations is strength point of this investigation.

Author Contributions: Conceptualization, A.M.I., D.K.B. and A.S.S.; methodology, A.S.B. and G.H.R.; software, A.M.I. and A.S.S.; validation, D.K.B. and G.H.R.; formal analysis, A.M.I.; investigation, A.S.B. and A.S.S.; resources, A.M.I.; data curation, D.K.B.; writing—original draft, A.M.I., D.K.B. and A.S.B.; Writing—review & editing, A.M.I., G.H.R. and A.S.S.; Supervision, A.M.I. All authors have read and agreed to the published version of the manuscript.

Funding: This study is funded by the Deputyship for Research and Innovation of the Saudi Ministry of Education via its funding for the PSAU Advanced Computational Intelligence and Intelligent Systems Engineering (ACIISE) Research Group, Project Number IF-PSAU-2022/01/22246.

Data Availability Statement: Data is unavailable due to privacy.

Conflicts of Interest: The authors declare no conflict of interest.

References

1. Pusppanathan, J.; Rahim, R.A.; Phang, F.A.; Mohamad, E.J.; Ayob, N.M.N.; Rahiman, M.H.F.; Seong, C.K. Single-plane dual-modality tomography for multiphase flow imaging by integrating electrical capacitance and ultrasonic sensors. *IEEE Sens. J.* **2017**, *17*, 6368–6377. [CrossRef]
2. Mohamad, E.; Rahim, R.; Rahiman, M.; Ameran, H.; Muji, S.; Marwah, O. Measurement and analysis of water/oil multiphase flow using electrical capacitance tomography sensor. *Flow Meas. Instrum.* **2016**, *47*, 62–70. [CrossRef]
3. Rahim, R.A.; Yunos, Y.M.; Rahiman, M.H.F.; Muji, S.Z.M.; Thiam, C.K.; Rahim, H.A. Optical tomography: Velocity profile measurement using orthogonal and rectilinear arrangements. *Flow Meas. Instrum.* **2012**, *23*, 49–55. [CrossRef]
4. Abouelwafa, M.S.A.; Kendall, E.J.M. The measurement of component ratios in multiphase systems using alpha-ray attenuation. *J. Phys. E Sci. Instrum.* **1980**, *13*, 341. [CrossRef]
5. Chen, T.-C.; Iliyasu, A.M.; Alizadeh, S.M.; Salama, A.S.; Eftekhari-Zadeh, E.; Hirota, K. The use of artificial intelligence and time characteristics in the optimization of the structure of the volumetric percentage detection system independent of the scale value inside the pipe. *Appl. Artif. Intell.* **2023**, *37*, 2166225.

6. Mayet, A.M.; Alizadeh, S.M.; Kakarash, Z.A.; Al-Qahtani, A.A.; Alanazi, A.K.; Grimaldo Guerrero, J.W.; Alhashimi, H.H.; Eftekhari-Zadeh, E. Increasing the Efficiency of a Control System for Detecting the Type and Amount of Oil Product Passing through Pipelines Based on Gamma-Ray Attenuation, Time Domain Feature Extraction, and Artificial Neural Networks. *Polymers* **2022**, *14*, 2852.
7. Peyvandi, R.G.; Rad, S.Z.I. Application of artificial neural networks for the prediction of volume fraction using spectra of gamma rays backscattered by three-phase flows. *Eur. Phys. J. Plus* **2017**, *132*, 511. [CrossRef]
8. Mayet, A.M.; Alizadeh, S.M.; Kakarash, Z.A.; Al-Qahtani, A.A.; Alanazi, A.K.; Alhashimi, H.H.; Eftekhari-Zadeh, E.; Nazemi, E. Introducing a Precise System for Determining Volume Percentages Independent of Scale Thickness and Type of Flow Regime. *Mathematics* **2022**, *10*, 1770.
9. Hanus, R.; Zych, M.; Petryka, L.; Jaszczur, M.; Hanus, P. Signals features extraction in liquid-gas flow measurements using gamma densitometry. Part 1: Time domain. *EPJ Web Conf.* **2016**, *114*, 02035. [CrossRef]
10. Hanus, R.; Zych, M.; Petryka, L.; Jaszczur, M.; Hanus, P. Signals features extraction in liquid-gas flow measurements using gamma densitometry. Part 2: Frequency domain. *EPJ Web Conf.* **2016**, *114*, 02036. [CrossRef]
11. Hanus, R.; Zych, M.; Kusy, M.; Jaszczur, M.; Petryka, L. Identification of liquid-gas flow regime in a pipeline using gamma-ray absorption technique and computational intelligence methods. *Flow Meas. Instrum.* **2018**, *60*, 17–23. [CrossRef]
12. Hanus, R.; Zych, M.; Petryka, L.; Świsulski, D.; Strzępowicz, A. Application of ANN and PCA to two-phase flow evaluation using radioisotopes. *EPJ Web Conf.* **2017**, *143*, 02033. [CrossRef]
13. Salgado, C.M.; Brandão, L.E.; Conti, C.C.; Salgado, W.L. Density prediction forpetroleum and derivatives by gamma-ray attenuation and artificial neural networks. *Appl. Radiat. Isot.* **2016**, *116*, 143–149. [CrossRef]
14. Salgado, W.L.; Dam, R.S.; Teixeira, T.P.; Conti, C.C.; Salgado, C.M. Application of artificial intelligence in scale thickness prediction on offshore petroleum using a gamma-ray densitometer. *Radiat. Phys. Chem.* **2020**, *168*, 108549. [CrossRef]
15. Salgado, C.M.; Brandão, L.E.; Schirru, R.; Pereira, C.M.; da Silva, A.X.; Ramos, R. Prediction of volume fractions in three-phase flows using nuclear technique and artificial neural network. *Appl. Radiat. Isot.* **2009**, *67*, 1812–1818. [CrossRef]
16. Salgado, C.M.; Pereira, C.M.; Schirru, R.; Brandão, L.E. Flow regime identification and volume fraction prediction in multiphase flows by means of gamma-ray attenuation and artificial neural networks. *Prog. Nucl. Energy* **2010**, *52*, 555–562. [CrossRef]
17. Khayat, O.; Afarideh, H. Design and simulation of a multienergy gamma ray absorptiometry system for multiphase flow metering with accurate void fraction and water-liquid ratio approximation. *Nukleonika* **2019**, *64*, 19–29. [CrossRef]
18. Affonso, R.R.W.; Dam, R.S.F.; Salgado, W.L.; da Silva, A.X.; Salgado, C.M. Flow regime and volume fraction identification using nuclear techniques, artificial neural networks and computational fluid dynamics. *Appl. Radiat. Isot.* **2020**, *159*, 109103. [CrossRef] [PubMed]
19. Shao, D.; Yan, Y.; Zhang, W.; Sun, S.; Sun, C.; Xu, L. Dynamic measurement of gas volume fraction in a CO_2 pipeline through capacitive sensing and data driven modelling. *Int. J. Greenh. Gas Control* **2020**, *94*, 102950. [CrossRef]
20. Basahel, A.; Sattari, M.A.; Taylan, O.; Nazemi, E. Application of Feature Extraction and Artificial Intelligence Techniques for Increasing the Accuracy of X-ray Radiation Based Two Phase Flow Meter. *Mathematics* **2021**, *9*, 1227. [CrossRef]
21. Taylan, O.; Sattari, M.A.; Essoussi, I.E.; Nazemi, E. Frequency Domain Feature Extraction Investigation to Increase the Accuracy of an Intelligent Nondestructive System for Volume Fraction and Regime Determination of Gas-Water-Oil Three-Phase Flows. *Mathematics* **2021**, *9*, 2091.
22. Mayet, A.M.; Nurgalieva, K.S.; Al-Qahtani, A.A.; Narozhnyy, I.M.; Alhashim, H.H.; Nazemi, E.; Indrupskiy, I.M. Proposing a high-precision petroleum pipeline monitoring system for identifying the type and amount of oil products using extraction of frequency characteristics and a MLP neural network. *Mathematics* **2022**, *10*, 2916. [CrossRef]
23. Balubaid, M.; Sattari, M.A.; Taylan, O.; Bakhsh, A.A.; Nazemi, E. Applications of discrete wavelet transform for feature extraction to increase the accuracy of monitoring systems of liquid petroleum products. *Mathematics* **2021**, *9*, 3215. [CrossRef]
24. Sattari, M.A.; Korani, N.; Hanus, R.; Roshani, G.H.; Nazemi, E. Improving the performance of gamma radiation based two phase flow meters using optimal time characteristics of the detector output signal extraction. *J. Nucl. Sci. Technol.* **2020**, *41*, 42–54.
25. Alanazi, A.K.; Alizadeh, S.M.; Nurgalieva, K.S.; Nesic, S.; Guerrero, J.W.G.; Abo-Dief, H.M.; Eftekhari-Zadeh, E.; Nazemi, E.; Narozhnyy, I.M. Application of neural network and time-domain feature extraction techniques for determining volumetric percentages and the type of two phase flow regimes independent of scale layer thickness. *Appl. Sci.* **2022**, *12*, 1336. [CrossRef]
26. Mayet, A.M.; Alizadeh, S.M.; Hamakarim, K.M.; Al-Qahtani, A.A.; Alanazi, A.K.; Grimaldo Guerrero, J.W.; Alhashim, H.H.; Eftekhari-Zadeh, E. Application of Wavelet Characteristics and GMDH Neural Networks for Precise Estimation of Oil Product Types and Volume Fractions. *Symmetry* **2022**, *14*, 1797. [CrossRef]
27. Mayet, A.M.; Chen, T.-C.; Alizadeh, S.M.; Al-Qahtani, A.A.; Qaisi, R.M.A.; Alhashim, H.H.; Eftekhari-Zadeh, E. Application of Artificial Intelligence for Determining the Volume Percentages of a Stratified Regime's Three-Phase Flow, Independent of the Oil Pipeline's Scale Thickness. *Processes* **2022**, *10*, 1996. [CrossRef]
28. Mayet, A.M.; Chen, T.-C.; Alizadeh, S.M.; Al-Qahtani, A.A.; Alanazi, A.K.; Ghamry, N.A.; Alhashim, H.H.; Eftekhari-Zadeh, E. Optimizing the Gamma Ray-Based Detection System to Measure the Scale Thickness in Three-Phase Flow through Oil and Petrochemical Pipelines in View of Stratified Regime. *Processes* **2022**, *10*, 1866. [CrossRef]
29. Mayet, A.M.; Chen, T.-C.; Ahmad, I.; Tag Eldin, E.; Al-Qahtani, A.A.; Narozhnyy, I.M.; Guerrero, J.W.G.; Alhashim, H.H. Application of Neural Network and Dual-Energy Radiation-Based Detection Techniques to Measure Scale Layer Thickness in Oil Pipelines Containing a Stratified Regime of Three-Phase Flow. *Mathematics* **2022**, *10*, 3544. [CrossRef]

30. Sattari, M.A.; Roshani, G.H.; Hanus, R.; Nazemi, E. Applicability of time-domain feature extraction methods and artificial intelligence in two-phase flow meters based on gamma-ray absorption technique. *Measurement* **2021**, *168*, 108474.
31. Sattari, M.A.; Roshani, G.H.; Hanus, R. Improving the structure of two-phase flow meter using feature extraction and GMDH neural network. *Radiat. Phys. Chem.* **2020**, *171*, 108725. [CrossRef]
32. Roshani, M.; Sattari, M.A.; Ali PJ, M.; Roshani, G.H.; Nazemi, B.; Corniani, E.; Nazemi, E. Application of GMDH neural network technique to improve measuring precision of a simplified photon attenuation based two-phase flowmeter. *Flow Meas. Instrum.* **2020**, *75*, 101804. [CrossRef]
33. Alamoudi, M.; Sattari, M.A.; Balubaid, M.; Eftekhari-Zadeh, E.; Nazemi, E.; Taylan, O.; Kalmoun, E.M. Application of Gamma Attenuation Technique and Artificial Intelligence to Detect Scale Thickness in Pipelines in Which Two-Phase Flows with Different Flow Regimes and Void Fractions Exist. *Symmetry* **2021**, *13*, 1198. [CrossRef]
34. Amoozegar, M.; Minaei-Bidgoli, B. Optimizing multi-objective PSO based feature selection method using a feature elitism mechanism. *Expert Syst. Appl.* **2018**, *113*, 499–514. [CrossRef]
35. Chen, T.-C.; Alizadeh, S.M.; Albahar, M.A.; Thanoon, M.; Alammari, A.; Guerrero, J.W.G.; Nazemi, E.; Eftekhari-Zadeh, E. Introducing the Effective Features Using the Particle Swarm Optimization Algorithm to Increase Accuracy in Determining the Volume Percentages of Three-Phase Flows. *Processes* **2023**, *11*, 236. [CrossRef]
36. Ullah, H.; Haq, Z.U.; Naqvi, S.R.; Khan MN, A.; Ahsan, M.; Wang, J. Optimization based comparative study of machine learning methods for the prediction of bio-oil produced from microalgae via pyrolysis. *J. Anal. Appl. Pyrolysis* **2023**, *170*, 105879. [CrossRef]
37. Kennedy, J.; Eberhart, R. Particle swarm optimization. In Proceedings of the ICNN'95-International Conference on Neural Networks, IEEE, Perth, Australia, 27 November–1 December 1995; Volume 4, pp. 1942–1948. [CrossRef]
38. Shi, Y.; Eberhart, R. A modified particle swarm optimizer. In Proceedings of the 1998 IEEE International Conference on Evolutionary Computation, IEEE, IEEE World Congress on Computational Intelligence (Cat. No. 98TH8360). Anchorage, AK, USA, 4–9 May 1998; pp. 69–73. [CrossRef]
39. Dabiri, H.; Farhangi, V.; Moradi, M.J.; Zadehmohamad, M.; Karakouzian, M. Applications of Decision Tree and Random Forest as Tree-Based Machine Learning Techniques for Analyzing the Ultimate Strain of Spliced and Non-Spliced Reinforcement Bars. *Appl. Sci.* **2022**, *12*, 4851. [CrossRef]
40. Zych, M.; Petryka, L.; Kępński, J.; Hanus, R.; Bujak, T.; Puskarczyk, E. Radioisotope investigations of compound two-phase flows in an open channel. *Flow Meas. Instrum.* **2014**, *35*, 11–15. [CrossRef]
41. Zych, M.; Hanus, R.; Wilk, B.; Petryka, L.; Świsulski, D. Comparison of noise reduction methods in radiometric correlation measurements of two-phase liquid-gas flows. *Measurement* **2018**, *129*, 288–295. [CrossRef]
42. Golijanek-Jędrzejczyk, A.; Mrowiec, A.; Hanus, R.; Zych, M.; Heronimczak, M.; Świsulski, D. Uncertainty of mass flow measurement using centric and eccentric orifice for Reynolds number in the range 10,000 $\leq$ Re $\leq$ 20,000. *Measurement* **2020**, *160*, 107851. [CrossRef]
43. Mayet, A.; Hussain, M. Amorphous WNx Metal for Accelerometers and Gyroscope. In Proceedings of the MRS Fall Meeting, Boston, MA, USA, 30 November–5 December 2014.
44. Mayet, A.; Hussain, A.; Hussain, M. Three-terminal nanoelectromechanical switch based on tungsten nitride—An amorphous metallic material. *Nanotechnology* **2016**, *27*, 035202. [CrossRef]
45. Shukla, N.K.; Mayet, A.M.; Vats, A.; Aggarwal, M.; Raja, R.K.; Verma, R.; Muqeet, M.A. High speed integrated RF–VLC data communication system: Performance constraints and capacity considerations. *Phys. Commun.* **2022**, *50*, 101492. [CrossRef]
46. Mayet, A.; Smith, C.E.; Hussain, M.M. Energy reversible switching from amorphous metal based nanoelectromechanical switch. In Proceedings of the 13th IEEE International Conference on Nanotechnology (IEEE-NANO 2013), Beijing, China, 5–8 August 2013; pp. 366–369.
47. Jedkare, E.; Shama, F.; Sattari, M.A. Compact Wilkinson power divider with multi-harmonics suppression. *AEU-Int. J. Electron. Commun.* **2020**, *127*, 153436. [CrossRef]
48. Artyukhov, A.V.; Isaev, A.A.; Drozdov, A.N.; Gorbyleva, Y.A.; Nurgalieva, K.S. The rod string loads variation during short-term annular gas extraction. *Energies* **2022**, *15*, 5045. [CrossRef]
49. Isaev, A.A.; Aliev, M.M.O.; Drozdov, A.N.; Gorbyleva, Y.A.; Nurgalieva, K.S. Improving the efficiency of curved wells' operation by means of progressive cavity pumps. *Energies* **2022**, *15*, 4259. [CrossRef]
50. Zhang, G.; Liu, R.; Ge, Y.; Mayet, A.M.; Chan, S.; Li, G.; Nazemi, E. Investigation on the Wilson Neuronal Model: Optimized Approximation and Digital Multiplierless Implementation. *IEEE Trans. Biomed. Circuits Syst.* **2022**, *16*, 1181–1190. [CrossRef] [PubMed]
51. Alanazi, A.K.; Alizadeh, S.M.; Nurgalieva, K.S.; Guerrero, J.W.G.; Abo-Dief, H.M.; Eftekhari-Zadeh, E.; Nazemi, E.; Narozhnyy, I.M. Optimization of X-ray tube voltage to improve the precision of two phase flow meters used in petroleum industry. *Sustainability* **2021**, *13*, 13622. [CrossRef]
52. Hosseini Tabatabaee, A.; Shama, F.; Sattari, M.A.; Veysifard, S. A miniaturized Wilkinson power divider with 12th harmonics suppression. *J. Electromagn. Waves Appl.* **2021**, *35*, 371–388. [CrossRef]
53. Mayet, A.M.; Alizadeh, S.M.; Nurgalieva, K.S.; Hanus, R.; Nazemi, E.; Narozhnyy, I.M. Extraction of Time-Domain Characteristics and Selection of Effective Features Using Correlation Analysis to Increase the Accuracy of Petroleum Fluid Monitoring Systems. *Energies* **2022**, *15*, 1986. [CrossRef]

54. Lalbakhsh, A.; Mohamadpour, G.; Roshani, S.; Ami, M.; Roshani, S.; Sayem, A.S.; Alibakhshikenari, M.; Koziel, S. Design of a compact planar transmission line for miniaturized rat-race coupler with harmonics suppression. *IEEE Access* **2021**, *9*, 129207–129217. [CrossRef]
55. Hookari, M.; Roshani, S.; Roshani, S. High-efficiency balanced power amplifier using miniaturized harmonics suppressed coupler. *Int. J. RF Microw. Comput. Aided Eng.* **2020**, *30*, e22252. [CrossRef]
56. Lotfi, S.; Roshani, S.; Roshani, S.; Gilan, M.S. Wilkinson power divider with band-pass filtering response and harmonics suppression using open and short stubs. *Frequenz* **2020**, *74*, 169–176. [CrossRef]
57. Jamshidi, M.; Siahkamari, H.; Roshani, S.; Roshani, S. A compact Gysel power divider design using U-shaped and T-shaped resonators with harmonics suppression. *Electromagnetics* **2019**, *39*, 491–504. [CrossRef]
58. Roshani, S.; Jamshidi, M.B.; Mohebi, F.; Roshani, S. Design and modeling of a compact power divider with squared resonators using artificial intelligence. *Wirel. Pers. Commun.* **2021**, *117*, 2085–2096. [CrossRef]
59. Roshani, S.; Azizian, J.; Roshani, S.; Jamshidi, M.B.; Parandin, F. Design of a miniaturized branch line microstrip coupler with a simple structure using artificial neural network. *Frequenz* **2022**, *76*, 255–263. [CrossRef]
60. Khaleghi, M.; Salimi, J.; Farhangi, V.; Moradi, M.J.; Karakouzian, M. Application of Artificial Neural Network to Predict Load Bearing Capacity and Stiffness of Perforated Masonry Walls. *CivilEng* **2021**, *2*, 48–67. [CrossRef]
61. Taylor, J.G. *Neural Networks and Their Applications*; John Wiley Sons Ltd.: Brighton, UK, 1996.
62. Gallant, A.R.; White, H. On learning the derivatives of an unknown mapping with multilayer feedforward networks. *Neural Netw.* **1992**, *5*, e129–e138. [CrossRef]
63. Song, X.; Zhang, Y.; Guo, Y.-N.; Sun, X.-Y.; Wang, Y.-L. Variablesize cooperative coevolutionary particle swarm optimization for feature selection on high-dimensional data. *IEEE Trans. Evol. Comput.* **2020**, *24*, 882–895. [CrossRef]
64. Tran, B.; Xue, B.; Zhang, M. Variable-length particle swarm optimization for feature selection on high-dimensional classification. *IEEE Trans. Evol. Comput.* **2019**, *23*, 473–487. [CrossRef]
65. Jain, I.; Jain, V.K.; Jain, R. Correlation feature selection based improved-Binary Particle Swarm Optimization for gene selection and cancer classification. *Appl. Soft Comput.* **2018**, *62*, 203–215. [CrossRef]

Disclaimer/Publisher's Note: The statements, opinions and data contained in all publications are solely those of the individual author(s) and contributor(s) and not of MDPI and/or the editor(s). MDPI and/or the editor(s) disclaim responsibility for any injury to people or property resulting from any ideas, methods, instructions or products referred to in the content.